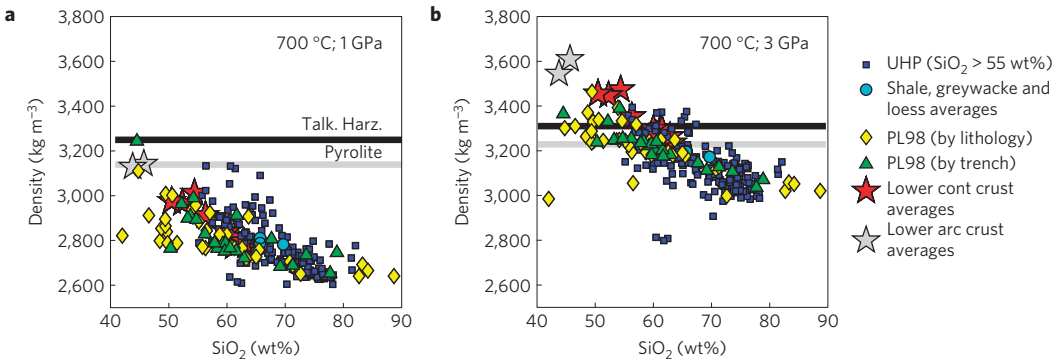

Figure 2 | Density of subducted sediments at UHP conditions. Density calculated at 700 °C and **a**, 1 GPa and **b**, 3 GPa as a function of SiO_2 content for compiled UHP metasedimentary compositions (dark blue squares), our estimates of average shale and greywacke, average loess, and the average of prior shale compositional averages (light blue circles), and subducting sediment delineated by lithology (yellow diamonds[30]) and location (green triangles[30]). Average lower continental and arc lower crust[50] are shown with red and grey stars, respectively. Black and grey horizontal lines show densities calculated for harzburgite[14] and pyrolite[35], respectively. Relative to the mantle wedge almost all sediment compositions are buoyant at 700 °C and pressures <3 GPa.

Thus, the apparent efficiency of recycling together with UHP metapelite compositions suggests that the sediment-melt signature in arcs is generated at >1,000 °C—significantly above the fluid-saturated sediment solidus. Temperatures greater than 1,000 °C are not reached on the slab top at pressures less than 5 GPa in even the hottest subduction-zone thermal models. Thus, we argue that the most likely location for the UHP metapelites to have reached temperatures >1,000 °C beneath volcanic arcs is within the mantle wedge. A possible example of this process is recorded by a peraluminous xenolith with oxygen isotopes indicative of a metasedimentary protolith from South Africa, which records peak metamorphic conditions of 1,200–1,300 °C and 4–5 GPa (that is, mantle wedge rather than subduction zone conditions)[27].

Timescale for the formation of sediment diapirs

Numerical modelling studies have shown the potential for subducting sediments to rise buoyantly into the mantle wedge[17,28,29]. However, these studies focused on systems in which the sediments are entrained in buoyant, hydrated mantle diapirs[17,28], or on very thick (>2 km) sediment layers[29], not representative of the thickness of sediment subducting to depth at modern arcs. Moreover, no studies have yet presented formal non-Newtonian scaling for sediment diapirs as a function of such key parameters as sediment thickness and density—preventing quantitative constraints on where and when sediment diapirs may form during subduction. Here we present a new, non-Newtonian scaling analysis for subducting sediments, to assess the timescale and depth at which a sediment layer may become unstable even in the absence of other sources of buoyancy (for example, a hydrated mantle layer).

To evaluate the intrinsic buoyancy of subducting sediments, we first calculated densities for the compiled UHP metapelites and averages of pelitic sediment compositions (ref. 30; Supplementary Information) and compared them to the density of the overlying mantle wedge (see Methods section). At 700 °C and pressures ≤3 GPa, almost all UHP rocks and sediment averages are buoyant with respect to the mantle wedge (Fig. 2). Further, for both warm (Cascadia) and cold (Izu-Bonin) slab-top geotherms[8] the density contrast between the overlying mantle and the average UHP metapelite is as much as $-200\,kg\,m^{-3}$ for all pressures up to 6 GPa (Fig. 3).

The timescale over which instabilities grow in a buoyant sediment layer is related to the relative viscosities of the sediment and overlying mantle, the viscous decay length in the mantle, and the buoyancy and thickness of the sediment layer[31–35]. We calculated instability times assuming a wet olivine rheology for the mantle wedge[36] that is 100× more viscous than the underlying

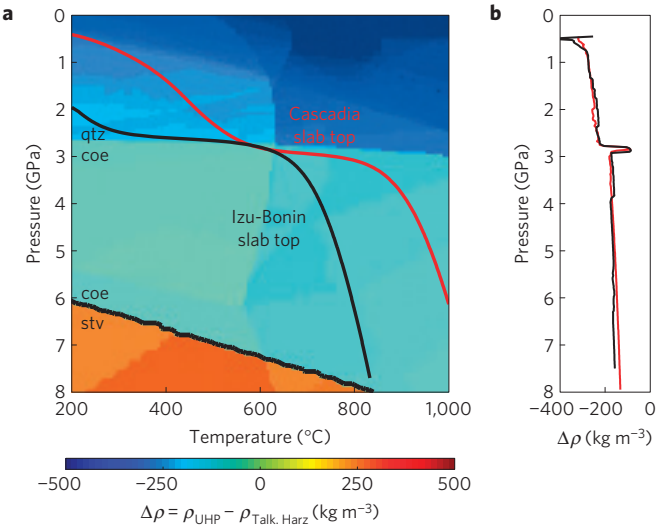

Figure 3 | Density of the average UHP metasediment along typical subduction zone geotherms. a, Density contrast between the average UHP metasedimentary composition and mantle wedge harzburgite[14] as a function of temperature and pressure. Thick red and black lines show slab-top geotherms for Cascadia and Izu-Bonin, respectively[8]. **b**, Density contrast as a function of pressure along the Cascadia (red) and Izu-Bonin (black) slab-top geotherms. Note that the density contrast is $\leq -200\,kg\,m^{-3}$ for all pressures <6 GPa.

sediment layer (Fig. 4, see Methods section). This viscosity contrast is appropriate for wet quartz[37] at temperatures between 600° and 800 °C. For a 500 m-thick sediment layer with a density contrast of $-200\,kg\,m^{-3}$ relative to the overlying mantle, the timescale for instability formation is <1 Myr and <10 kyr at temperatures of 700 °C and 800 °C, respectively (Fig. 4a and grey region in Fig. 4b). Moreover, any sediment layer thicker than ~100 m will become unstable on timescales shorter than 1 Myr at temperatures ≤1,000 °C (Fig. 4a).

The conditions for diapir formation in a given subduction zone can be determined by integrating the instability time along the slab-top pressure–temperature–time (P–T–t) path until the amplitude of the instability exceeds the initial thickness of the sediment layer. To illustrate this approach, the P–T conditions at which diapirs form in Cascadia and Izu–Bonin were calculated assuming a sediment thickness of 500 m (stars on the black and red curves in Fig. 4b). In both cases, diapirs form between ~675°–750 °C and

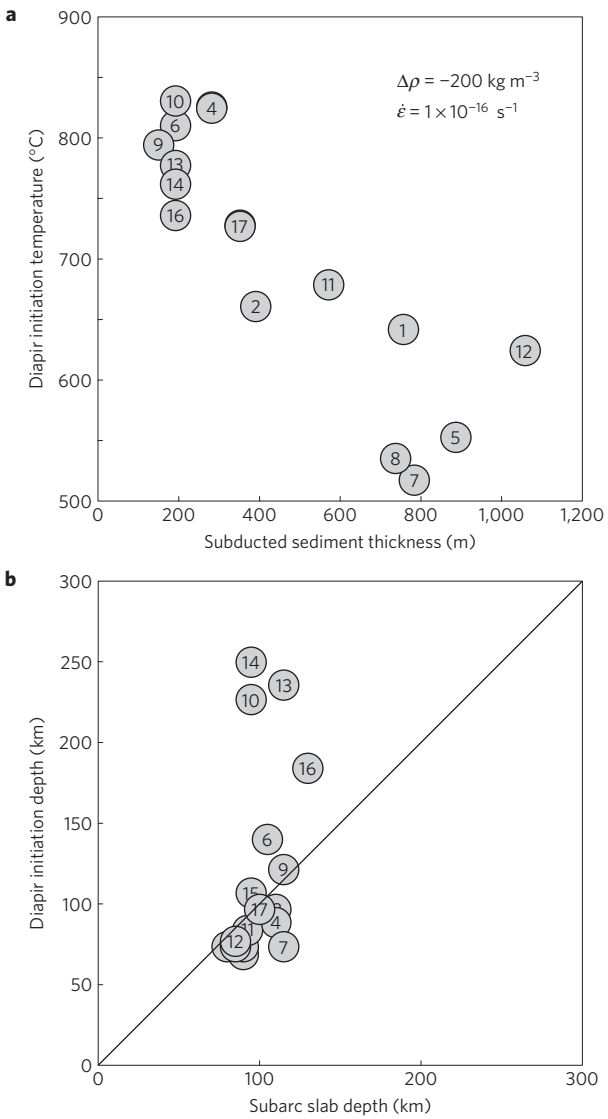

Figure 4 | Calculated timescale for the initiation of a sediment diapir. **a**, Instability time versus temperature and sediment layer thickness for a density contrast of −200 kg m^{-3}, background strain-rate of 10^{-16} s^{-1}, and initial perturbation amplitude 33% of the layer thickness. For typical subduction rates, diapirs form between 2 and 4 GPa if the instability time is ≤1 Myr (thick black contour). **b**, Location of diapir formation (stars) on slab-top geotherms for Cascadia (red) and Izu-Bonin (black) assuming a sediment thickness of 500 m. Grey region shows instability times for background strain-rates ranging from 10^{-14} to 10^{-18} s^{-1}. Diapirs are predicted to form at 685 °C and ~2.3 GPa in Cascadia and 730 °C and 3.2 GPa in Izu-Bonin.

Figure 5 | Summary of conditions for sediment diapir formation in global subduction zones. a, Diapir initiation temperature versus sediment layer thickness[30], and **b**, diapir initiation depth versus subarc slab depth (as compiled in ref. 8) calculated for 17 slab-top geotherms[8]. Subducting sediment layer thicknesses are corrected for compaction to a density of 2,800 kg m^{-3}. Numbers (in order of increasing slab thermal parameter) correspond to subduction zones: 1—Cascadia, 2—Nankai, 3—Mexico, 4—Colombia-Ecuador, 5—SC Chile, 6—Kyushu, 7—N. Sumatra, 8—Alaska, 9—N. Chile, 10—N. Costa Rica, 11—Aleutians, 12—N. Hikurangi, 13—Mariana, 14—Tonga-Kermadec, 15—Kamchatka, 16—Izu, and 17—NE Japan.

2.2–3.0 GPa, with a slightly greater formation depth in Izu–Bonin due to the colder incoming slab.

Based on slab-top geotherms[8] and the estimated thickness of the downgoing sediment layer[38,39], we explored the conditions of diapir formation for 17 different subduction systems (Fig. 5). For all subduction systems, diapirs form between 500° and 850 °C (Fig. 5a), with higher temperatures corresponding to thinner sediment layers because instability growth rates scale positively with layer thickness[31,34,35]. These temperatures are near the fluid-saturated sediment solidus, but significantly below the ~1,050 °C required to deplete metasediments in Th, Sr, Pb and Nd (Fig. 1). Thus, we conclude that diapirs of buoyant metasediment detach from the downgoing slab and rise buoyantly into the mantle wedge, where they are heated to temperatures >1,000–1,100 °C.

A key difference between these results and previous work is that we predict diapiric rise for sediment layers with wet quartz rheology that are as thin as 100 m, whereas Currie *et al.* (ref. 29) concluded that buoyant 'wet quartz' layers less than 1-km thick would not form diapirs unless the magnitude of the density contrast was >200 kg m^{-3}. Thus, because the sediment layer thickness is <1 km for all but one of the subduction zones in Fig. 5a, Currie *et al.*[29] would not predict instabilities for any of these unless the density contrast was consistently significantly greater than 200 kg m^{-3}. Such high density contrasts are inconsistent with our calculated density contrasts for metasediments at UHP conditions (Fig. 2).

Our calculations predict that in all but four subduction zones with very thin sediment layers, diapirs form within ±40 km of

the slab depth below the arc (Fig. 5b). This indicates that partial melts derived from metasedimentary diapirs rising through the hot mantle wedge could easily be incorporated into the arc melting regime. The details of these calculations are sensitive to the slab-top geotherm. Subduction-zone thermal models have evolved considerably over the past 10 years, incorporating effects such as temperature- and stress-dependent rheology, decoupling between the downgoing slab and overriding plate, and variable slab geometry[5–8]. However, many potentially important effects, including thermal advection associated with melts and fluids and thermal/mechanical erosion of the upper plate, have yet to be incorporated into these models. Furthermore, our calculations assume a steady-state thickness of the subducting sediment layer, whereas temporal variations are likely. Thus, although a robust conclusion of our analysis is that diapirs form at temperatures $<\sim$850 °C and near the depth of arc-magma genesis, further details on their formation will require improved subduction-zone thermal models.

Implications for arc volcanism and mantle wedge dynamics

Based on our scaling analysis (see Methods section), diapirs will form from a sediment layer 250–500 m thick with an along-arc spacing of 4–8 km and diameters of 3–4 km. The diffusion time required to raise the temperature to $\geq$1,000 °C at the centre of a sphere with these dimensions is on the order of 10^4 yr assuming that the surrounding mantle is at 1,350 °C. This is more than an order of magnitude faster than the transit time of a similarly sized diapir through the mantle wedge based on analogue experiments[40], and implies that the sediments would thermally equilibrate and undergo extensive melting before reaching the top of the mantle wedge. However, sediment diapirs of this size would comprise only $\sim$0.1% of the mantle wedge by volume, and thus would have a negligible influence on the time-averaged wedge temperature and the kinematics of mantle flow. Furthermore, given their small size they would be difficult to detect seismically. This contrasts with models of buoyant 'cold plumes' that have been proposed to arise from much thicker layers of hydrated mantle located above or below the downgoing plate[17], and/or foundering of dense arc lower crust[41], both of which could significantly alter wedge temperatures and mantle flow patterns. Furthermore, the calculated spacing of sediment diapirs is significantly less than the 30–100 km spacing of most arc volcanoes[32], indicating that the spacing of sediment diapirs is not the underlying cause of the spacing of volcanic centres in arcs.

The high H_2O/Ce and H_2O/K ratios observed in some arcs[11–13] (for example, Tonga, where the rapid convergence rate and great age of the subducting plate combine to yield relatively low slab top temperatures in thermal models) are difficult to explain as the result of extensive melting of metasedimentary diapirs. Instead, it is possible that the subduction component in these arcs is transported from the slab top by means of aqueous fluids or near-solidus, small-degree partial melts, rather than produced by partial melting of diapirs within the mantle wedge. In our study, diapirs are predicted to initiate late, behind the volcanic arc, in the relatively cold Tonga–Kermadec and Mariana–Izu–Bonin arc systems (Fig. 5), where the subducting sediment layer is thin, the recycled sediment signature is muted[2,24], and recycling efficiencies are relatively low (see Supplementary Information).

Finally, the efficient removal and recycling of sediments into the mantle wedge will influence volatile fluxes into the deep mantle at subduction zones. In the case of H_2O, only a small fraction of sediment H_2O ($\sim$5%) is subducted to postarc depths[42], and thus the formation of sediment diapirs will have a relatively minor influence on the total recycling efficiency. However, decarbonation reactions occur at higher temperatures than dehydration reactions, implying that a greater fraction of carbonate rocks may be transported to postarc depths[43–45]. Currently, global estimates of the slab-derived CO_2 by decarbonation[43] are significantly less than CO_2 drawdown by silicate weathering[46,47]. Thus, sediment diapirs provide an efficient mechanism for recycling these carbonates into the arc melting regime, and may provide a mechanism to balance the global carbon cycle.

Methods

Sediment densities were calculated using Perple_X 2007 (ref. 48) and thermodynamic data[49] and solution models[42] appropriate for arc mineral assemblages. We assumed 2 wt% H_2O for all compositions, which is representative of the amount of H_2O retained in subducting metasediments at 700 °C and 3 GPa (ref. 42). Based on the calculated density contrast between the average UHP composition and mantle wedge harzburgite[14] at pressures <4 GPa (Fig. 3b) we assume a value of $-200\,kg\,m^{-3}$ for all instability calculations.

The rate of instability growth is sensitive to the viscosity contrast between the buoyant layer and overlying half-space. To determine the viscosity ratio we calculated viscosities for wet quartz[37] and wet olivine[36] ($C_{OH} = 2{,}500\,H/10^6$ Si) over a range of temperatures and strain rates. For strain rates of 10^{-16}–$10^{-17}\,s^{-1}$ (typical of the slab–wedge interface in numerical models of wedge corner flow with non-Newtonian rheology[5,8]), wet olivine is 2–3 orders of magnitude more viscous than wet quartz at 600–800 °C (the approximate temperature range over which diapirs form). Before 2001, geodynamic studies of density instability assumed that mobile, buoyant crustal layers were more viscous than the adjacent mantle half space, which was then assumed to be inviscid. By contrast, in the scenarios considered here metasediment is much weaker than the mantle. Thus, instability times were calculated based on non-Newtonian growth rates for a 'weak' buoyant layer (layer: half-space viscosity ratio = 1:100) and an assumed background strain rate[35].

Instability growth rates are sensitive to the length-scale over which viscosity decreases in the overlying half-space[31,34]. For wet olivine, a slab-top temperature of 700 °C, and a vertical temperature gradient of 20–40 °C km^{-1} across the slab-wedge interface[6], the viscous decay length is $\sim$0.5–1.5 km (ref. 34). The instability growth rates were then calculated based on the ratio of the viscous decay length to the sediment layer thickness[35]. Finally, the spacing of the instabilities was determined from the wavenumber of the fastest growth rate.

Received 20 December 2010; accepted 24 June 2011; published online 7 August 2011

References

1. Kessel, R., Schmidt, M. W., Ulmer, P. & Pettke, T. Trace element signature of subduction-zone fluids, melts and supercritical liquids at 120–180 km depth. *Nature* **437,** 724–727 (2005).
2. Plank, T. & Langmuir, C. H. Tracing trace elements from sediment input to volcanic output at subduction zones. *Nature* **362,** 739–743 (1993).
3. Elliott, T., Plank, T., Zindler, A., White, W. & Bourdon, B. Element transport from slab to volcanic front at the Mariana arc. *J. Geophys. Res.* **102,** 14991–15019 (1997).
4. Hawkesworth, C. J., Turner, S. P., McDermott, F., Peate, D. W. & van Calsteren, P. U–Th isotopes in arc magmas: Implications for element transfer from the subducted crust. *Science* **276,** 551–555 (1997).
5. van Keken, P. E., Kiefer, B. & Peacock, S. M. High-resolution models of subduction zones: Implications for mineral dehydration reactions and the transport of water into deep mantle. *Geochem. Geophys. Geosyst.* **3,** 1056 (2002).
6. Kelemen, P. B., Rilling, J. L., Parmentier, E. M., Mehl, L. & Hacker, B. R. in *Inside the Subduction Factory* Vol. 138 (ed. Eiler, J.) 293–311 (Geophysical Monograph, AGU, 2003).
7. Peacock, S. M. *et al.* Thermal structure of the Costa Rica–Nicaragua subduction zone. *Phys. Earth Planet. Inter.* **149,** 187–200 (2005).
8. Wada, I. & Wang, K. Common depth of slab-mantle decoupling: Reconciling diversity and uniformity of subduction zones. *Geochem. Geophys. Geosyst.* **10,** Q10009 (2009).
9. Nichols, G. T., Wyllie, P. J. & Stern, C. R. Subduction zone melting of pelagic sediments constrained by melting experiments. *Nature* **371,** 785–788 (1994).
10. Schmidt, M. W., Vielzeuf, D. & Auzanneau, E. Melting and dissolution of subducting crust at high pressures: The key role of white mica. *Earth Planet. Sci. Lett.* **228,** 65–84 (2004).
11. Plank, T., Cooper, L. B. & Manning, C. E. Emerging geothermometers for estimating slab surface temperatures. *Nature Geosci.* **2,** 611–615 (2009).
12. Hermann, J. & Rubatto, D. Accessory phase control on the trace element signature of sediment melts in subduction zones. *Chem. Geol.* **265,** 512–526 (2009).
13. Hermann, J. & Spandler, C. J. Sediment melts at sub-arc depths: An experimental study. *J. Petrol.* **49,** 717–740 (2008).
14. Kelemen, P. B., Hanghøj, K. & Greene, A. R. in *The Crust* Vol. 3 (ed. Rudnick, R. L.) 593–659 (Treatise on Geochemistry, Elsevier, 2003).
15. Castro, A. & Gerya, T. V. Magmatic implications of mantle wedge plumes: Experimental study. *Lithos* **103,** 138–148 (2008).

16. Yin, A. *et al.* Early paleozoic tectonic and thermomechanical evolution of ultrahigh-pressure (UHP) metamorphic rocks in the northern Tibetan plateau, northwest China. *Int. Geol. Rev.* **49,** 681–716 (2007).
17. Gerya, T. V. & Yuen, D. A. Rayleigh–Taylor instabilities from hydration and melting propel 'cold plumes' at subduction zones. *Earth Planet. Sci. Lett.* **212,** 47–62 (2003).
18. Becker, H., Jochum, K. P. & Carlson, R. W. Trace element fractionation during dehydration of eclogites from high-pressure terranes and the implications for element fluxes in subduction zones. *Chem. Geol.* **163,** 65–99 (2000).
19. Bebout, G. E., Ryan, J. G., Leeman, W. P. & Bebout, A. E. Fractionation of trace elements by subduction-zone metamorphism—effect of convergent-margin thermal evolution. *Earth Planet. Sci. Lett.* **171,** 63–81 (1999).
20. Busigny, V., Cartigny, P., Philippot, P., Ader, M. & Javoy, M. Massive recycling of nitrogen and other fluid-mobile elements (K, Rb, Cs, H) in a cold slab environment: Evidence from HP to UHP oceanic metasediments of the Schistes Lustrés nappe (western Alps, Europe). *Earth Planet. Sci. Lett.* **215,** 27–42 (2003).
21. Hermann, J. & Green, D. H. Experimental constraints on high pressure melting in subducted crust. *Earth Planet. Sci. Lett.* **188,** 149–168 (2001).
22. Thomsen, T. B. & Schmidt, M. W. Melting of carbonated pelites at 2.5–5.0 GPa, silicate–carbonatite liquid immiscibility, and potassium–carbon metasomatism of the mantle. *Earth Planet. Sci. Lett.* **267,** 17–31 (2008).
23. Johnson, M. C. & Plank, T. Dehydration and melting experiments constrain the fate of subducted sediments. *Geochem. Geophys. Geosyst.* **1,** 1007 (1999).
24. Klimm, K., Blundy, J. D. & Green, T. H. Trace element partitioning and accessory phase saturation during H_2O-saturated melting of basalt with implications for subduction zone chemical fluxes. *J. Petrol.* **49,** 523–553 (2008).
25. Massonne, H-J., Kennedy, A., Nasdala, L. & Theye, T. Dating of zircon and monazite from diamondiferous quartzofeldspathic rocks of the Saxonian Erzgebirge. *Mineral. Mag.* **71,** 407–425 (2007).
26. Skora, S. & Blundy, J. High-pressure hydrous phase relations of radiolarian clay and implications for the involvement of subducted sediment in arc magmatism. *J. Petrol.* **51,** 2211–2243 (2010).
27. Sharp, Z. D., Essene, E. J. & Smyth, J. R. Ultra-high temperatures from oxygen isotope thermometry of a coesite-sanidine grospydite. *Contrib. Mineral. Petrol.* **122,** 358–370 (1992).
28. Gorczyk, W., Gerya, T. V., Connolly, J. A. D., Yuen, D. A. & Rudolph, M. Large-scale rigid-body rotation in the mantle wedge and its implications for seismic tomography. *Geochem. Geophys. Geosyst.* **7,** Q05018 (2006).
29. Currie, C. A., Beaumont, C. & Huismans, R. S. The fate of subducted sediments: A case for backarc intrusion and underplating. *Geology* **35,** 1111–1114 (2007).
30. Plank, T. & Langmuir, C. H. The chemical composition of subducting sediment and its consequences for the crust and mantle. *Chem. Geol.* **145,** 325–394 (1998).
31. Houseman, G. A. & Molnar, P. Gravitational (Rayleigh–Taylor) instability of a layer with non-linear viscosity and convective thinning of continental lithosphere. *Geophys. J. Int.* **128,** 125–150 (1997).
32. Marsh, B. D. Island arc development: Some observations, experiments, and speculations. *J. Geol.* **87,** 687–713 (1979).
33. Whitehead, J. A. Jr & Luther, D. S. Dynamics of laboratory diapir and plume models. *J. Geophys. Res.* **80,** 705–717 (1975).
34. Conrad, C. P. & Molnar, P. The growth of Rayleigh–Taylor-type instabilities in the lithosphere for various rheological and density structures. *Geophys. J. Int.* **129,** 95–112 (1997).
35. Jull, M. & Kelemen, P. B. On the conditions for lower crustal convective instability. *J. Geophys. Res.* **106,** 6423–6446 (2001).
36. Hirth, G. & Kohlstedt, D. L. in *Inside the Subduction Factory* Vol. 138 (ed. Eiler, J.) 83–105 (Geophysical Monograph, AGU, 2003).
37. Hirth, G., Teyssier, C. & Dunlap, W. J. An evaluation of quartzite flow laws based on comparisons between experimentally and naturally deformed rocks. *Int. J. Earth Sci.* **90,** 77–87 (2001).
38. Clift, P. D. & Vannucchi, P. Controls on tectonic accretion versus erosion in subduction zones: Implications for the origin and recycling of the continental crust. *Rev. Geophys.* **42,** RG2001 (2004).
39. von Huene, R. & Scholl, D. W. Observations at convergent margins concerning sediment subduction, subduction erosion, and the growth of continental crust. *Rev. Geophys.* **29,** 279–316 (1991).
40. Hall, P. S. & Kincaid, C. Diapiric flow at subduction zones: A recipe for rapid transport. *Science* **292,** 2472–2475 (2001).
41. Behn, M. D., Hirth, G. & Kelemen, P. B. Trench-parallel anisotropy produced by foundering of arc lower crust. *Science* **317,** 108–111 (2007).
42. Hacker, B. R. H_2O subduction beyond arcs. *Geochem. Geophys. Geosyst.* **9,** Q03001 (2008).
43. Gorman, P. J., Kerrick, D. M. & Connolly, J. A. D. Modeling open system metamorphic decarbonation of subducting slabs. *Geochem. Geophys. Geosyst.* **7,** Q04007 (2006).
44. Kerrick, D. M. & Connolly, J. A. D. Metamorphic devolatilization of subducted oceanic metabasalts: Implications for seismicity, arc magmatism and volatile recycling. *Earth Planet. Sci. Lett.* **189,** 19–29 (2001).
45. Molina, J. F. & Poli, S. Carbonate stability and fuid composition in subducted oceanic crust: An experimental study on H_2O–CO_2-bearing basalts. *Earth Planet. Sci. Lett.* **176,** 295–310 (2000).
46. Varekamp, J. C. & Thomas, E. Volcanic and anthropogenic contributions to global weathering budgets. *J. Geochem. Expl.* **62,** 149–159 (1998).
47. Berner, R. A. & Kothavala, Z. GEOCARB III: A revised model of atmospheric CO_2 over Phanerozoic time. *Am. J. Sci.* **301,** 182–204 (2001).
48. Connolly, J. A. D. Computation of phase equilibria by linear programming: A tool for geodynamic modeling and its application to subduction zone decarbonation. *Earth Planet. Sci. Lett.* **236,** 524–541 (2005).
49. Holland, T. & Powell, R. Calculation of phase relations involving haplogranitic melts using an internally consistent thermodynamic dataset. *J. Petrol.* **42,** 673–683 (2001).
50. Behn, M. D. & Kelemen, P. B. The relationship between seismic P-wave velocity and the composition of anhydrous igneous and meta-igneous rocks. *Geochem. Geophys. Geosyst.* **4,** 1041 (2003).

Acknowledgements

We thank S. McLennan for assistance in compiling shale and greywacke compositions, I. Wada for providing her slab top thermal models, and C. Conrad, A. Shaw, T. Plank and J. Connolly for insightful conversations. Funding for this work was provided by NSF and WHOI's Deep Ocean Exploration Institute.

Author contributions

M.D.B., P.B.K. and G.H. performed the instability calculations. B.R.H., P.B.K. and H-J.M. compiled the UHP metapelite database. P.B.K. compiled the shale and greywacke database and produced the geochemical figures. M.D.B. took the lead in preparing the manuscript with significant input from all authors.

Additional information

The authors declare no competing financial interests. Supplementary information accompanies this paper on www.nature.com/naturegeoscience. Reprints and permissions information is available online at http://www.nature.com/reprints. Correspondence and requests for materials should be addressed to M.D.B.